Photo-controlled Chirality Transfer and FRET Effects based on Pseudo[3]rotaxane

Hong-guang Fu,[a] Heng-Yi Zhang,[a] Hao-Yang Zhang,[a] and Yu Liu*[a]

[a] *Department of Chemistry, State Key Laboratory of Elemento-Organic Chemistry, Nankai University, Tianjin 300071, P. R. China*

Table of Contents

Experimental Procedures

All the reagents and solvents were commercially available and used as received unless otherwise specified purification. Compounds, 3[a], were prepared according to the literatures procedure. Column chromatography was performed on 200-300 mesh silica gel.

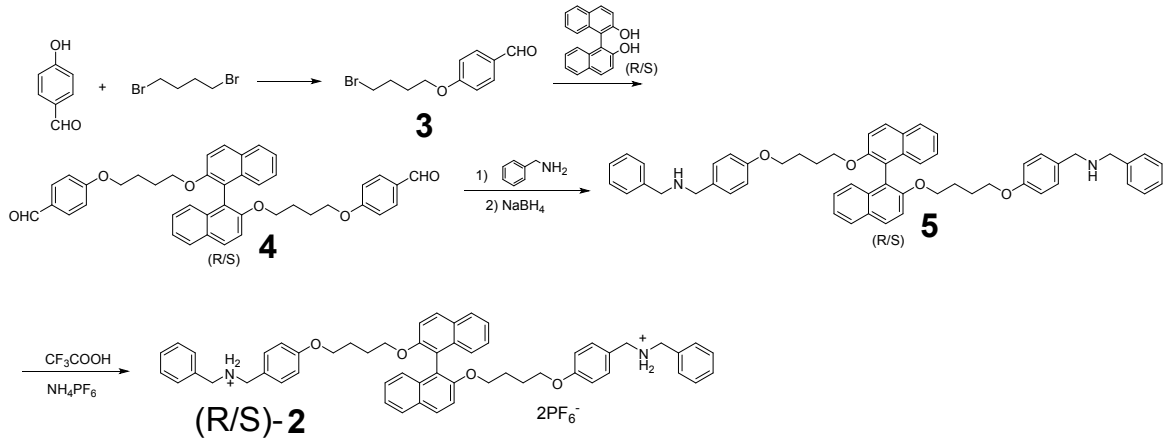

Scheme S1. Synthetic route of (*R/S*)-**2**.

Preparation of 4. Complex **3** (309 mg, 1.2 mmol), 1,1′-Bi-2-naphthol (114.5 mg, 0.4 mmol), and K_2CO_3 (550 mg, 4 mmol) were suspended in anhydrous MeCN (20 mL). The reaction mixture was heated to reflux under argon atmosphere and stirred for 24 h. After cooling down to r. t., the reaction mixture was filtered off and washed with CH_2Cl_2 (100 mL). The filtrate was concentrated under reduced pressure, which was further purified by column chromatography (SiO2, hexane : ethyl acetate = 6:1) to yield the product 4. (199 mg, 82%). ^{1}H NMR (400 MHz, $CDCl_3$, 298 K) δ: 9.86 (s, 2H), 7.91 (d, *J* = 9.0 Hz, 2H), 7.83 (d, *J* = 8.1 Hz, 2H), 7.77 (d, *J* = 8.7 Hz, 4H), 7.40 (d, *J* = 9.0 Hz, 2H), 7.34–7.28 (m, 2H), 7.20 (q, *J* = 8.6 Hz, 4H), 6.74 (d, *J* = 8.6 Hz, 4H), 4.18–4.02 (m, 4H), 4.00–3.90 (m, 2H), 3.56–3.40 (m, 4H). ^{13}C NMR (101 MHz, CDCl3) δ: 190.96 , 164.32 , 154.69, 134.41 , 132.12 , 130.00 , 129.74 , 129.68, 128.20 , 126.56 , 125.74 , 124.02 , 121.17 , 116.29 , 114.95 , 69.68 , 67.74 , 60.64. m/z calcd for $C_{42}H_{39}O_6^+$: 639.2747 ($M+H^+$), found:639.2743.

Preparation of 5 and (*R/S*)-2. A solution of **4** (1277.5 mg, 2.0 mmol) and benzylamine (437.35 mg, 4.0 mmol) in EtOH (50 mL) was heated under reflux for 12 h. After the reaction mixture was cooled to r.t., $NaBH_4$ (0.76 g, 20.0 mmol) was added to this solution in small portions, and the reaction mixture stirred at r.t. for another 12 h. The solvent was evaporated under reduced pressure and the residue was partitioned between CH_2Cl_2 (50 mL) and water (50 mL). The aqueous layer was further washed with CH_2Cl_2 (3 × 100 mL). The organic phases were combined and dried over anhydrous $MgSO_4$. Filtration, followed by evaporation

gave a white solid which was subjected to column chromatography (SiO_2, CH_2Cl_2 : MeOH = 100:3). Pure **5** was obtained as a white solid (1.26 g, 80%). ^{1}H NMR (400 MHz, $CDCl_3$) δ 7.89 (d, *J* = 9.0 Hz, 2H), 7.82 (d, *J* = 8.1 Hz, 2H), 7.38 (d, *J* = 9.0 Hz, 2H), 7.34–7.11 (m, 20H), 6.66 (d, *J* = 8.4 Hz, 4H), 4.01 (dt, *J* = 9.3, 5.9 Hz, 2H), 3.90 (dt, *J* = 13.7, 6.6 Hz, 2H), 3.76 (s, 4H), 3.70 (s, 4H), 3.45 (t, *J* = 6.2 Hz, 4H), 1.98 (s,2H), 1.61–1.43 (m, 4H), 1.31 (qq, *J* = 13.3, 6.5 Hz, 4H). ^{13}C NMR (101 MHz, $CDCl_3$) δ: 158.27 , 154.66 , 140.39 , 134.36 , 132.12 , 129.58 , 129.50 , 129.48 , 128.65 , 128.44 , 128.13, 127.21 , 126.43 , 125.69, 123.83 , 69.50 , 67.20 , 53.72 , 53.18 , 52.71 , 26.06 , 25.61. m/z calcd for $C_{56}H_{58}N_2O_6^{2+}$: 411.2199 (M + $2H^+$), found:411.2195. Then compound **5** (100 mg, 0.127 mmol) was dissolved in dry CH_2Cl_2 (20 mL) and TFA (0.19 mL, 0.3 mmol) TFA (0.32 mL, 5.0 mmol) was added at room tempeature. After the solution stirred for 2 h under argon atmosphere, the solvent was removed under vacuum. The residue was dissolved in MeOH, and then saturated NH_4PF_6 (20 mL, aq) was added and stirred for several minutes to yield a yellow creamy solid. The residue was extracted by CH_2Cl_2. The organic layer was washed by H_2O for three times and dried over anhydrous Na_2SO_4, and thesolvent was removed under vacuum to give the compound (R/S)-**2** (123 mg, 90%). ^{1}H NMR (400 MHz, CD_3CN) δ 8.01 (d, *J* = 8.9 Hz, 2H), 7.91 (d, *J* = 7.9 Hz, 2H), 7.58–7.42 (m, 12H), 7.34 (dd, *J* = 17.3, 7.9 Hz, 6H), 7.21 (t, *J* = 7.2 Hz, 2H), 7.04 (d, *J* = 8.2 Hz, 2H), 6.79 (d, *J* = 8.0 Hz, 4H), 4.20 (d, *J* = 16.7 Hz, 8H), 4.14–3.97 (m, 4H), 1.64–1.47 (m, 8H), 1.39 (d, *J* = 12.0 Hz, 8H). ^{13}C NMR (101 MHz, CD_3CN) δ 211.12, 203.99 , 160.76 , 155.26 , 134.74, 132.61 , 131.31 , 130.98 , 130.56 , 130.17 , 130.10 , 129.91, 128.85, 127.13 , 125.65, 124.43 , 122.81 , 120.79 , 116.48 , 115.55 , 69.74, 68.04 , 61.99 , 51.99 , 51.86 , 50.32 , 28.10. m/z calcd for (**2**-$2PF_6$)$^{2+}$: 411.2199 , found:411.2195.

Measurements

NMR spectroscopy. ^{1}H and ^{13}C NMR spectra and 2D ROESY were recorded on a Brucker AV400 spectrometer.

Fluorescence spectroscopy. Steady-state fluorescence spectra were recorded in a conventional quartz cell (light path 10 mm) on a Varian Cary Eclipse equipped with a Varian Cary single-cell peltier accessory to control temperature.

UV/Vis spectroscopy. UV/Vis spectra and the optical transmittance were recorded in a quartz cell (light path 10 mm) on a Shimadzu UV-3600 spectrophotometer equipped with a PTC-348WI temperature controller.

ESI-MS spectroscopy. Electrospray ionization mass spectra (ESI-MS) were measured by Agilent 6520 Q-TOF-MS.

CD spectroscopy. CD spectra were recorded on a BioLogic MOS500 spectropolarimeter in a quartz cell of 10 mm light path.

Switch experiments. The switch experiments were carried out using a photochemical reaction apparatus with a 500W Hg lamp.

Theoretical calculation section. To further understand the mechanism of the surprising ICD signals, density functional theory (DFT) and time-dependent density functional theory (TD-DFT) calculations were performed by Gaussian16.[b] The geometry optimization were carried out at B3LYP-GD3[c-d] / 6-31G(d,p) [e] level with symmetry constraint. TD-DFT and natural transition orbitals (NTOs) were calculated using the M06-2X-GD3[d,f] and 6-311G(d,p)[e] basis set in chloroform using the integral equation formalism polarizable continuum model (IEF-PCM).[g]As a comparison, model molecules $\mathbf{1_{mod}}$ and $\mathbf{2_{mod}}$ (Scheme.S22) were also calculated.

Figures

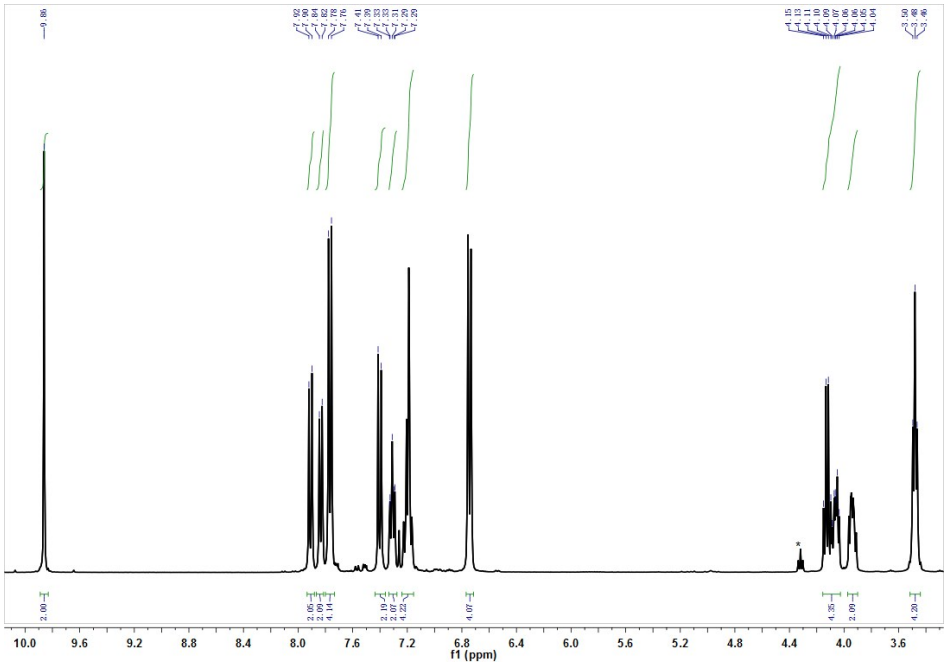

Figure S1. ^{1}H NMR (400 MHz) spectrum of **4** in $CDCl_3$ at 25 °C.

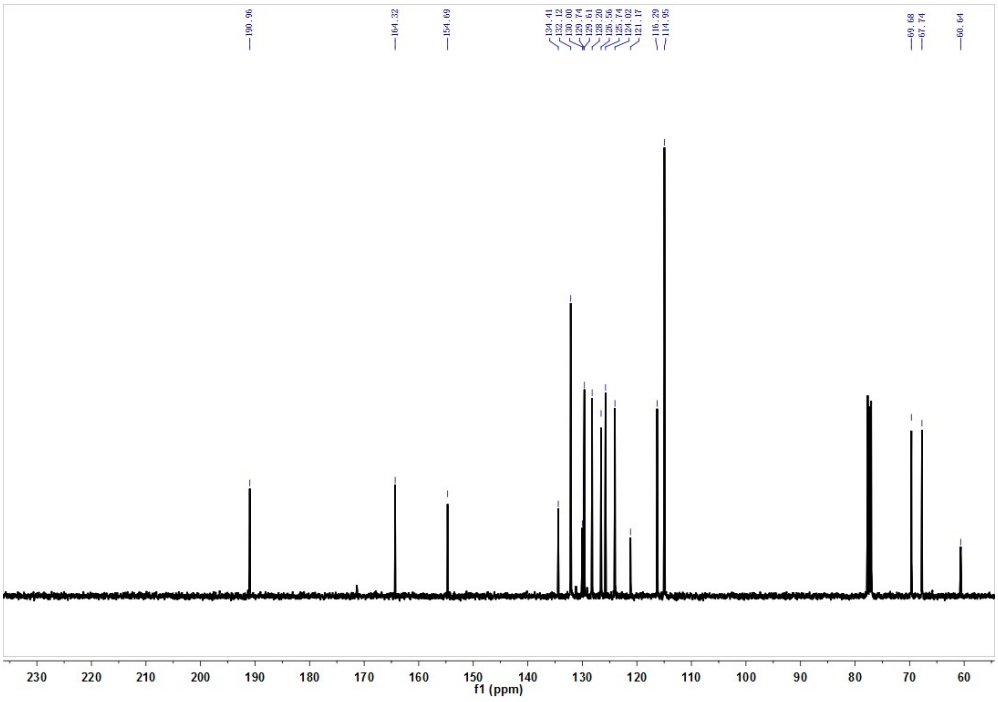

Figure S2. ^{13}C NMR (101 MHz) spectrum of **4** in $CDCl_3$ at 25 °C.

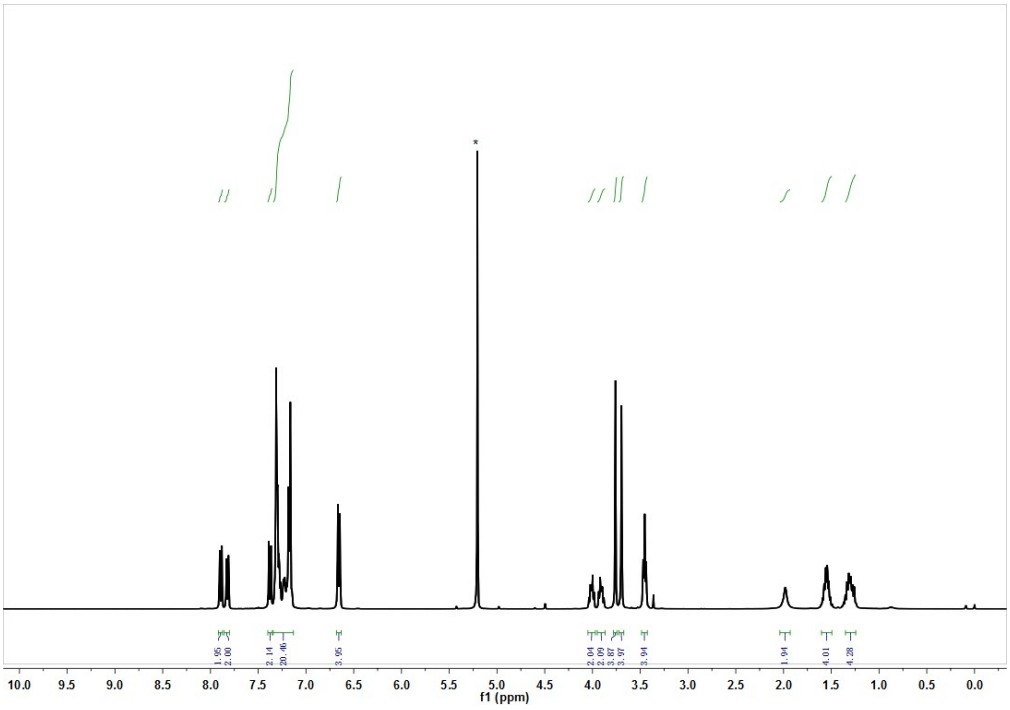

Figure S3. ^{1}H NMR (400 MHz) spectrum of **5** in $CDCl_3$ at 25 °C.

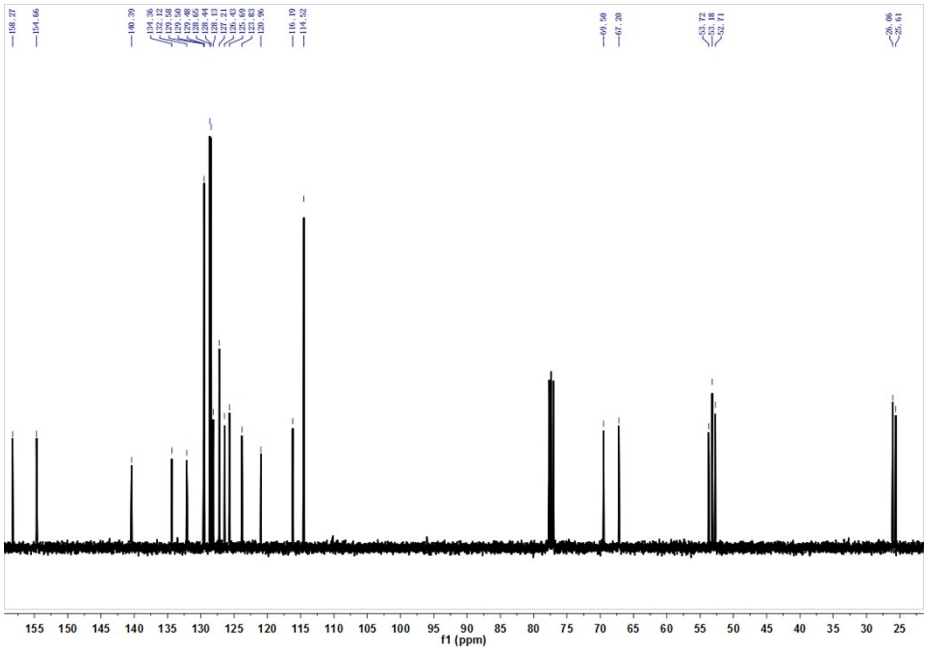

Figure S4. ^{13}C NMR (101 MHz) spectrum of **5** in $CDCl_3$ at 25 °C.

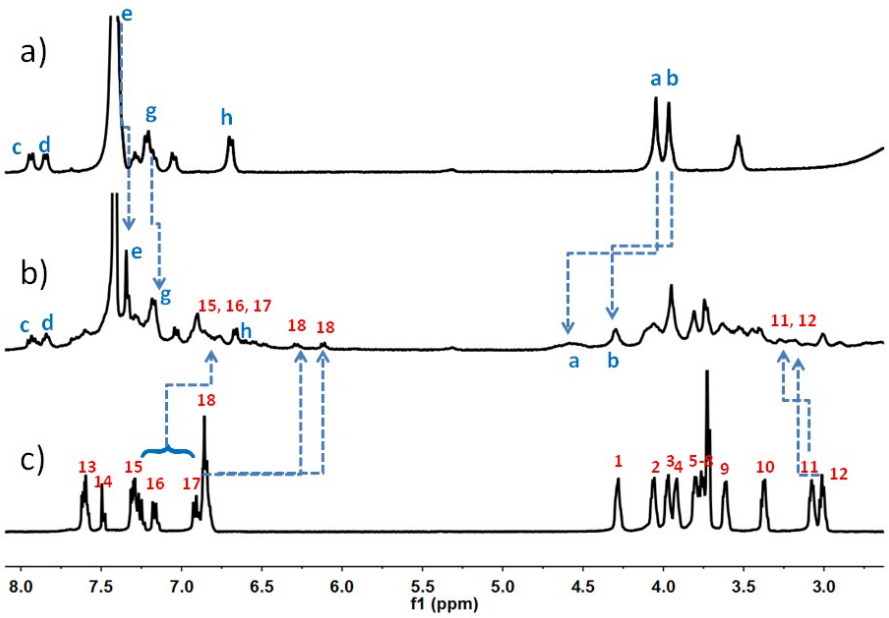

Figure S5. ^{1}H NMR spectra (400 MHz, $CDCl_3/CD_3CN$ = 2:1, 298 K, [(*S*)-**2**] = [**1**] = 1 mM) of (a) free guest (*S*)-**2**, (b) an equimolar mixture of (*S*)-**2** and **1**, and (c) free crown ether host **1**. for the full proton labeling, see Scheme 1.

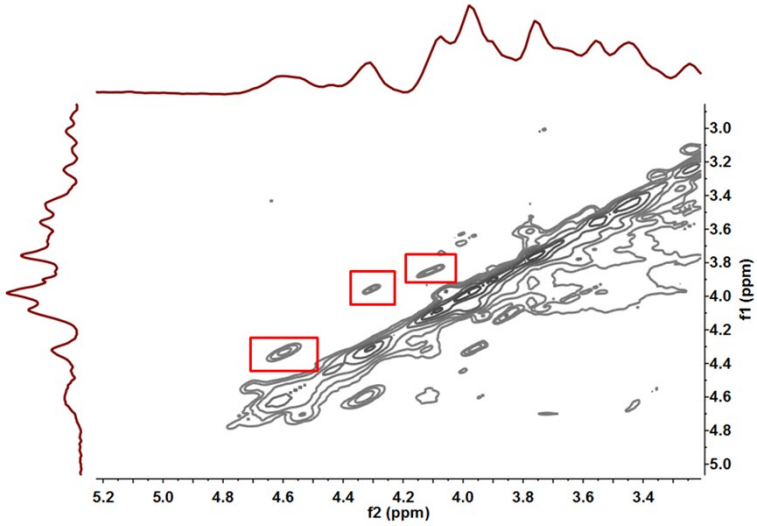

Figure S6. Selected regions of the ROESY 2D NMR spectrum (400 MHz, $CDCl_3/CD_3CN$ = 2:1) of (*R*)-**2**@**1**.

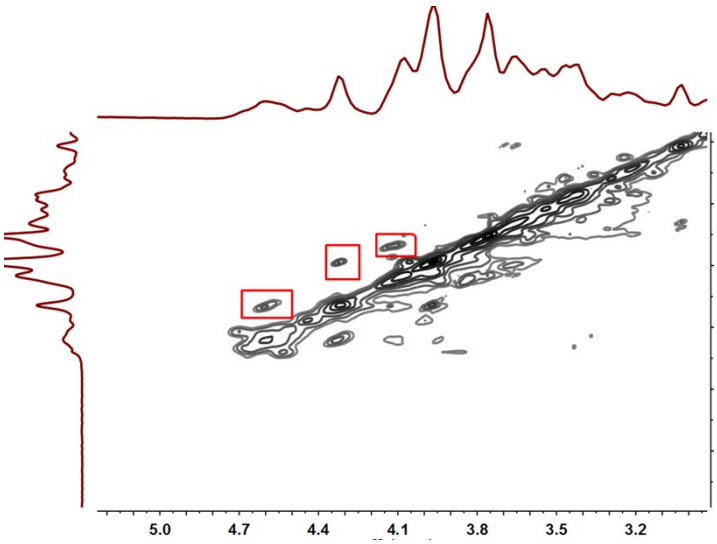

Figure S7. Selected regions of the ROESY 2D NMR spectrum (400 MHz, $CDCl_3/CD_3CN$ = 2:1) of (*S*)-**2**@**1**.

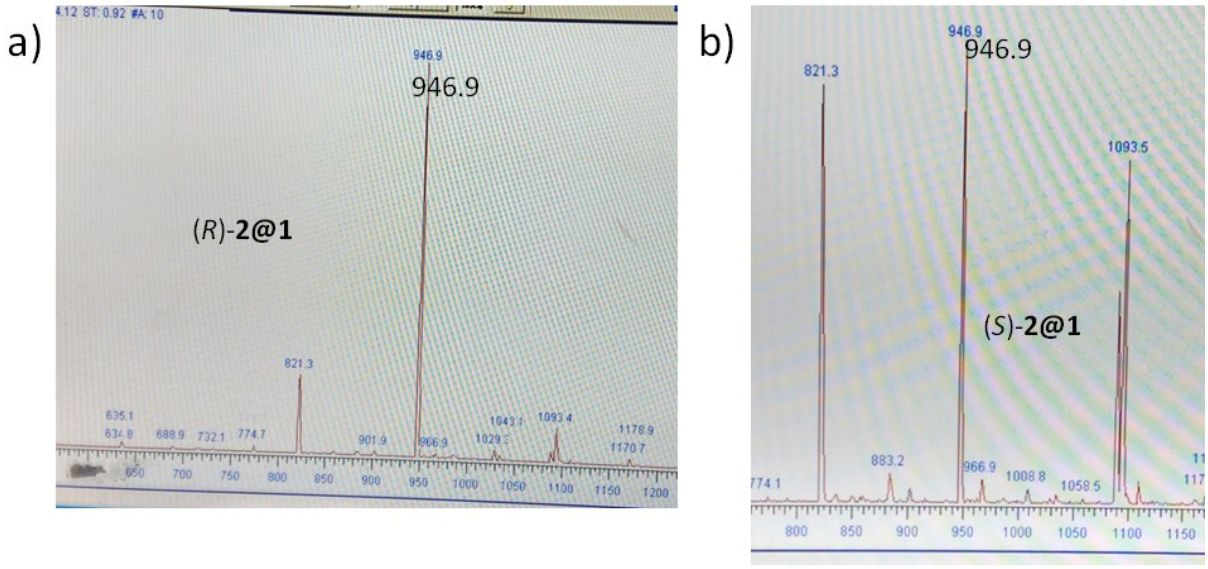

Figure S8. ESI-MS (low resolution) spectrum of a) (*R*)-**2**@**1**, b) (*S*)-**2**@**1** in $CHCl_3/CH_3CN$ (2:1) at 298 K. The peak at m/z = 946.6 is assigned to the $[(R/S)\text{-}\mathbf{2@1}]^{2+}$.

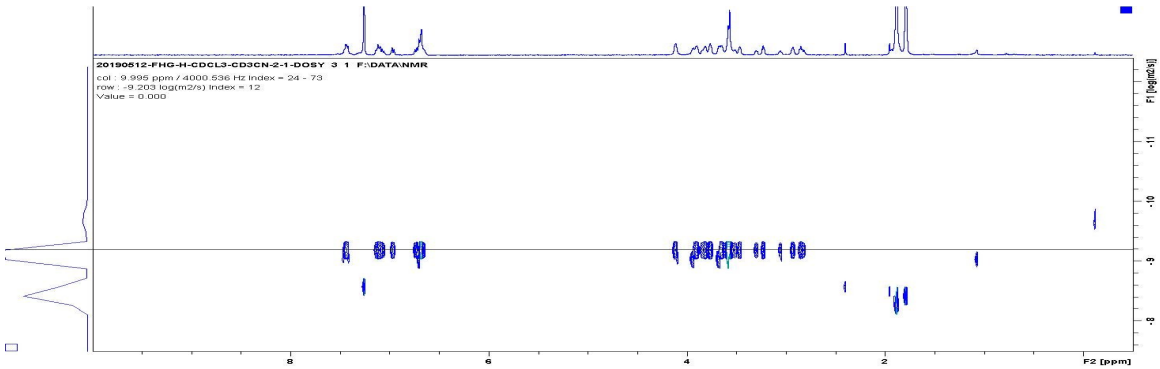

Figure S9. DOSY-NMR spectrum (400 MHz, $CDCl_3/CD_3CN$ = 2:1, 298 K) of **1** (1 mM), plotted using the log values of the diffusion constant.

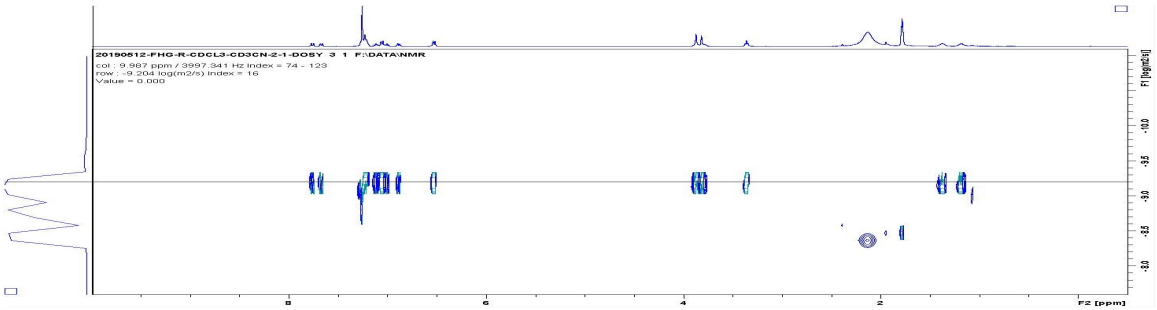

Figure S10. DOSY-NMR spectrum (400 MHz, $CDCl_3/CD_3CN$ = 2:1, 298 K) of (*R*)-**2** (1 mM), plotted using the log values of the diffusion constant.

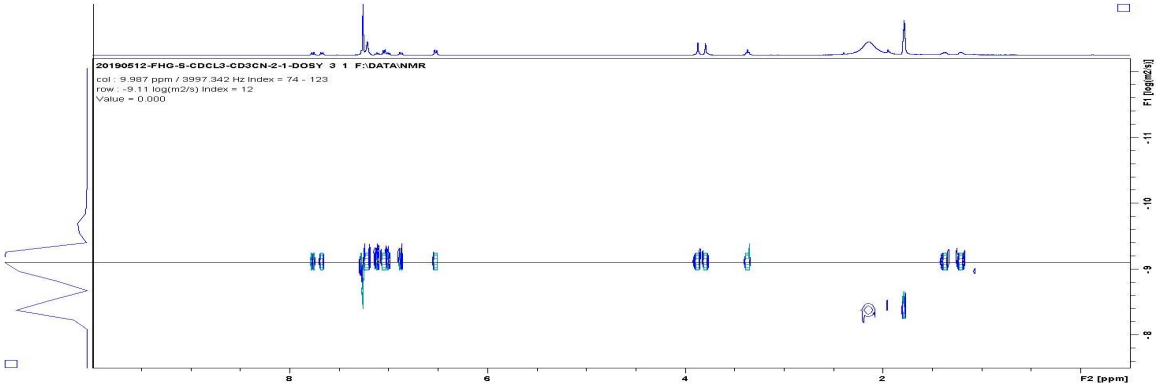

Figure S11. DOSY-NMR spectrum (400 MHz, $CDCl_3/CD_3CN$ = 2:1, 298 K) of (*S*)-**2** (1mM), plotted using the log values of the diffusion constant.

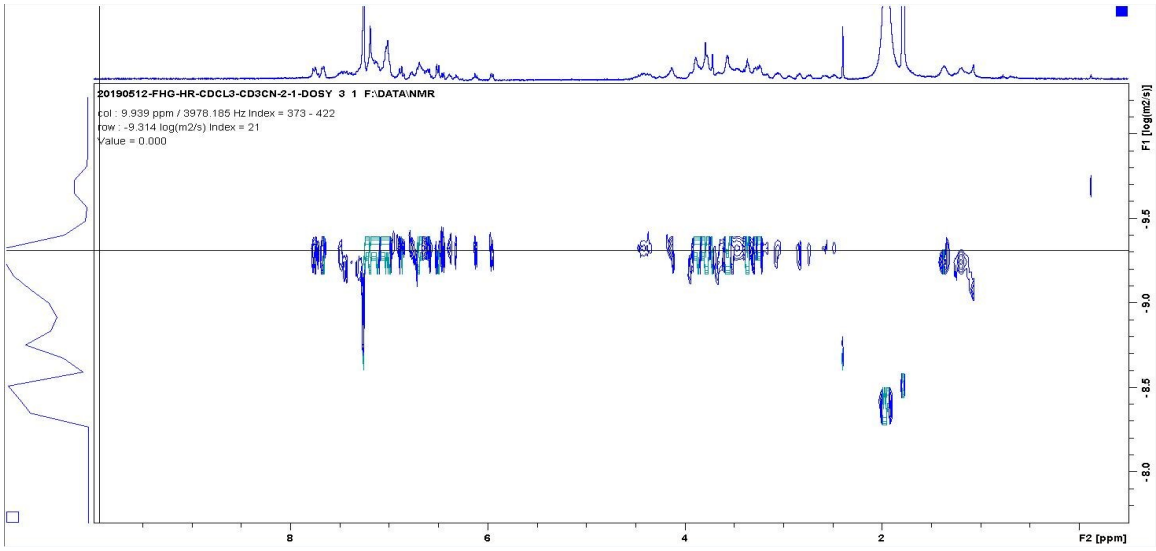

Figure S12. DOSY-NMR spectrum (400 MHz, $CDCl_3/CD_3CN$ = 2:1, 298 K) of (*R*)-**2**@**1** (1 mM), plotted using the log values of the diffusion constant.

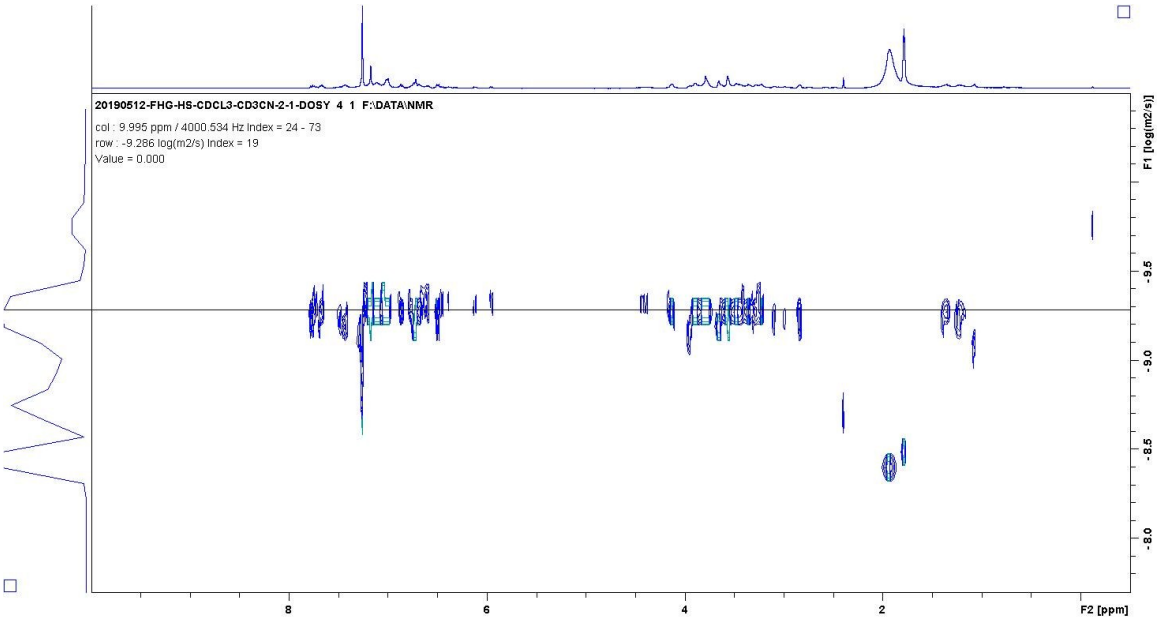

Figure S13. DOSY-NMR spectrum (400 MHz, $CDCl_3/CD_3CN$ = 2:1, 298 K) of (*S*)-**2**@**1** (1 mM), plotted using the log values of the diffusion constant.

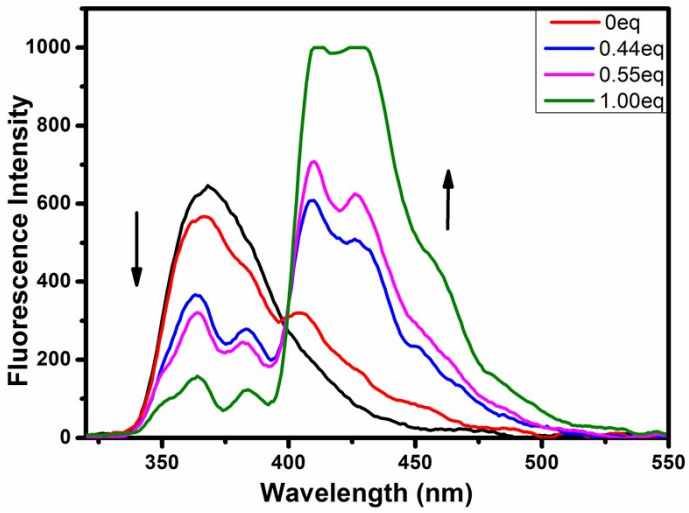

Figure S14. Fluorescence spectra of supramolecular assembly of **1** and (*R*)-**2** (6.0×10^{-5} M) with the addition of **1** (λ_{ex} = 305 nm).

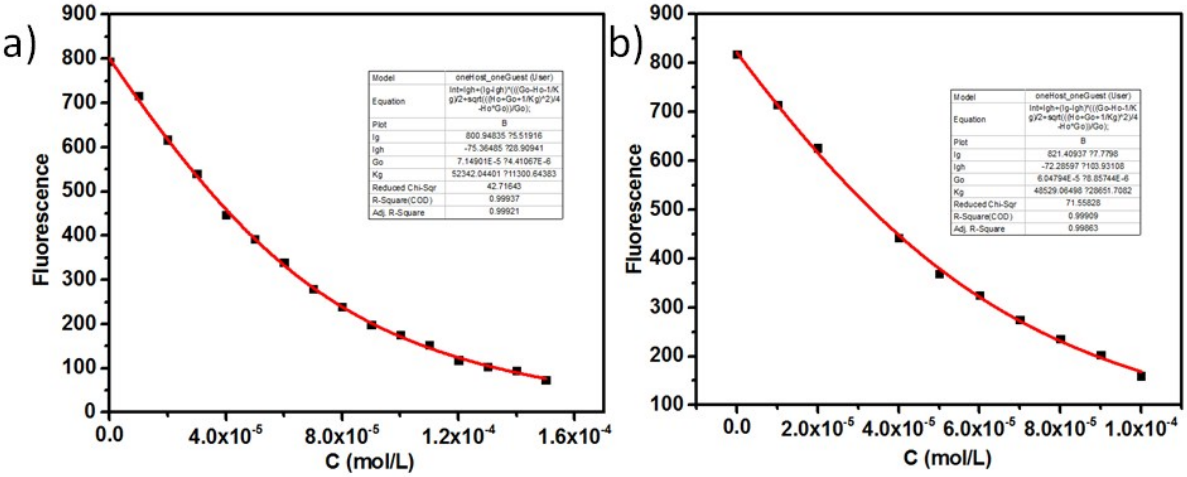

Figure S15. Nonlinear least-squares analysis of the emission (F, λ = 365 nm) of a) (*R*)-**2**@**1**, b) (*S*)-**2**@**1** to calculate the complex binding constant a) K = 5.2 × 10^4 M^{-1}, b) K = 4.9 × 10^4 M^{-1}.

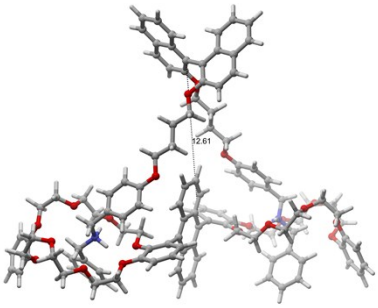

Figure S16. The optimized structure the assembly (*R*)-**2**@**1**[h].

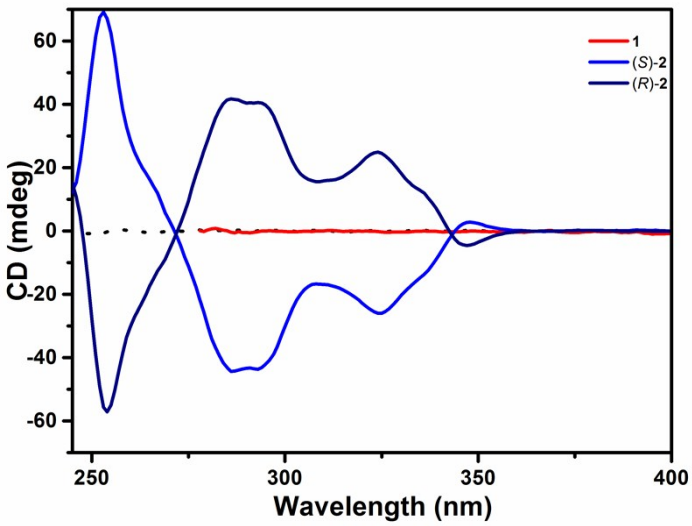

Figure S17. Circular dichroism spectra of (*R*)-**2**, (*S*)-**2**, **1** at 0.01m M.

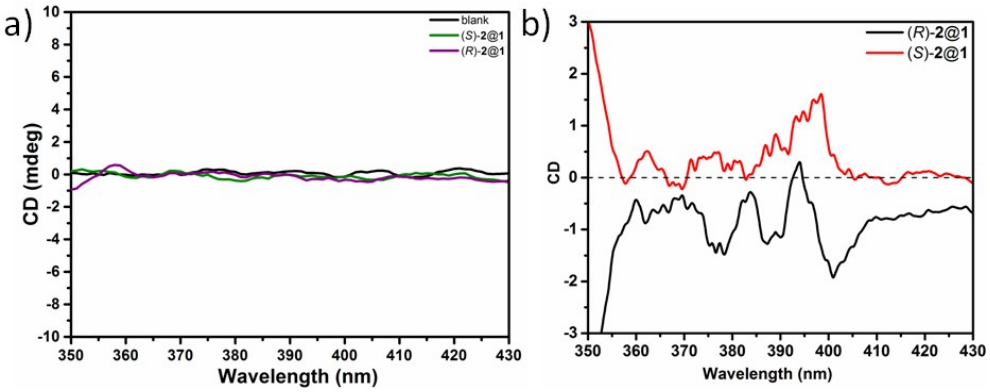

Figure S18. a) Circular dichroism spectra of (*R/S*)-**2**@**1** after irritated at 365 nm for 10 h，b) Circular dichroism spectra of a) after heated at 100°C for 10 h under N_2.

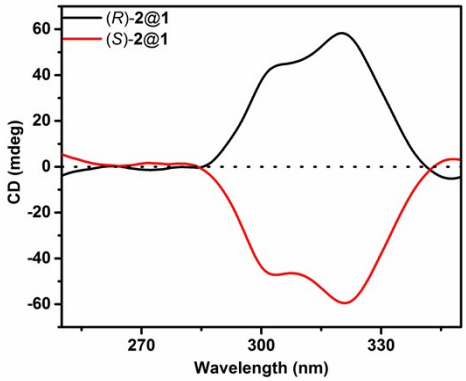

Figure S19. Circular dichroism spectra of (*R/S*)-**2**@**1** from 250 to 350 nm.

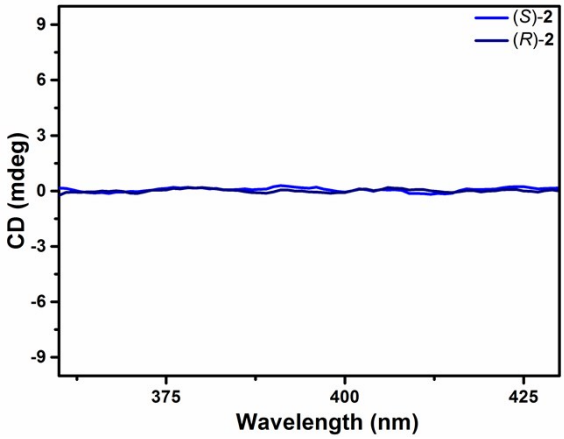

Figure S20. Circular dichroism spectra of (*R/S*)-**2** from 360 to 430 nm.

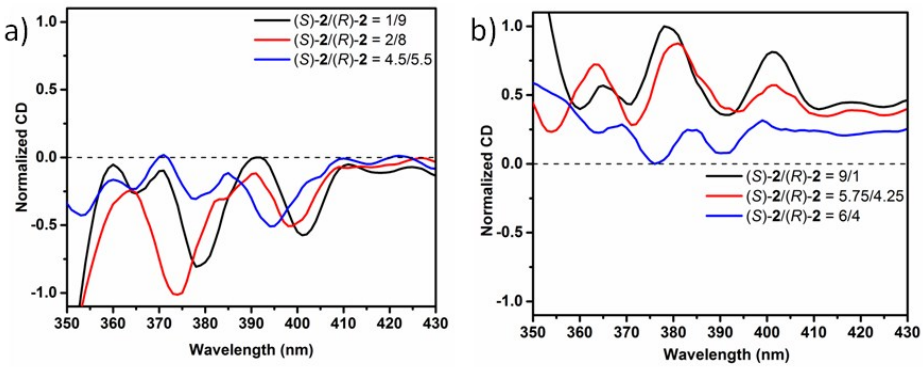

Figure S21. Normalized induced circular dichroism spectra of a), (*S*)-**2**/(*R*)-**2**= 1/9，2/8，4.5/5.5. b), (*S*)-**2**/(*R*)-**2**= 9/1, 5.75/4.25, 6/4. in $CHCl_3/CH_3CN$ at 298 k ([1] = [(*R*)-**2** + (*S*)-**2**] = 0.3 mM).

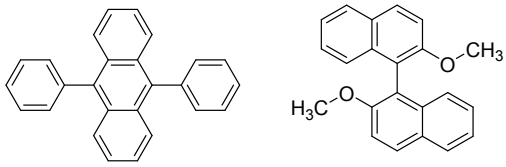

1$_{mod}$ **2**$_{mod}$

Scheme S22. The model molecules **1**$_{mod}$ and **2**$_{mod}$ of host and guest.

According to the simulation of electronic circular dichroism (ECD) spectrum by TD-DFT, we found that the signal of the excited state S_2 was opposite to the signal in the shorter-wavelength region for the assembly (*R*)-**2**@**1**, which was consistent with the experimental results. The NTOs calculation shown that the excited state S_2 was related to the transition local excitation in anthracene and charge-transfer excitation from guest to host (Table.S1 and Figure.S25). To be noted, there is a signal of S_2 whose direction is the same as the signal in shorter-wavelength region, but it is not shown in experiment. We think it is the result of vibration racemization. When the benzene ring is perpendicular to the anthracene ring, the chromophore is D_{2h} symmetry, and there is no CD signal due to no chirality. When the benzene ring rotated along the anthracene ring, the symmetry plane disappears and the symmetry of the chromophore group beecome D_2. The D_2 chromophore has CD signals accompanying its enantiomer has opposite CD signals.(Table.S2 and Figure.S23). Based on the Franck-Condon principle, the rate of the electron transition is much larger than the rate of molecular vibration. If the probability of molecular vibration to the two opposite directions is equal, the CD signal of local excitation will not be observed. However, for the excited state S_2 of the assembly, the vibration racemization will not occur at CT when the signal of LE disappear, but the strength of signal will decrease sharply in S_2. Moreover, we notice that the symmetry of the phase of the occupied orbital of the CT in S_2 is not similar with that of main transition in S_4 (Figure.S24), which may be the result of the selectivity of the orbital

symmetry in transition, and it is also the reason of that the exhibited ICD signals in anthracene were opposite to that of (S)-2 or (R)-2 in binaphthyl.

Table S1. Important electronic excited states and their NTOs analysis for (*R*)-**2**@**1** and (*R*)-**2**$_{mod}$.

Complex	Electronic transition	λ	Energy	R_{vel}	Assignment (H = HOMO, L = LUMO)
(*R*)-**2**@**1**	$S_0 \rightarrow S_1$	376.95nm	3.2891eV	20.5426	(0.70)H-1→L
	$S_0 \rightarrow S_2$	315.01nm	3.9359eV	-1.2265	(0.44)H-11→L
					(0.17)H-4→L
					(0.48)H-1→L+2
	$S_0 \rightarrow S_3$	298.82nm	4.1492eV	39.7861	(-0.26)H-2→L+3
					(0.63)H→L+1
					(0.11)H→L+21
	$S_0 \rightarrow S_4$	288.20nm	4.3020eV	66.7046	(-0.15)H-6→L+1
					(0.13)H-3→L+3
					(-0.11)H-3→L+17
					(-0.38)H-2→L+1
					(-0.11)H-2→L+21
					(0.50)H→L+3
					(0.16)H→L+17
(**R**)-**2**$_{mod}$	$S_0 \rightarrow S_1$	296.62nm	4.1798eV	-12.0321	(-0.35)H-1→L+1
					(0.57)H→L
					(-0.12)H→L+3
	$S_0 \rightarrow S_2$	289.33nm	4.2852eV	75.9631	(-0.15)H-3→L
					(-0.10)H-3→L+3
					(0.13)H-2→L+1
					(-0.12)H-2→L+2
					(-0.38)H-1→L
					(0.11)H-1→L+3
					(0.50)H→L+1
					(0.14)H→L+2

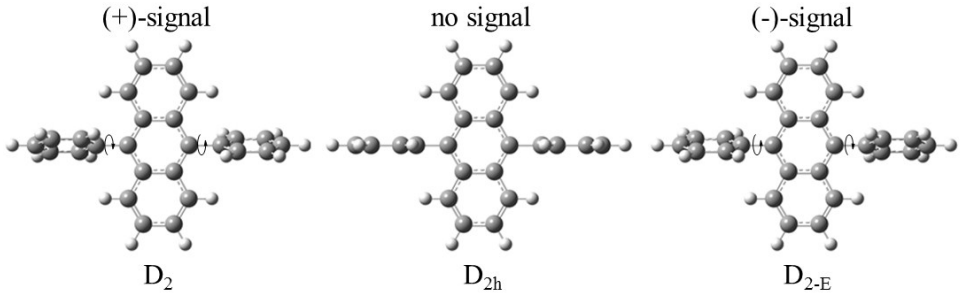

Figure S23. The direction of rotation and signal of **1**$_{mod}$-D_{2h}, **1**$_{mod}$-D_2 and its' enantiomer **1**$_{mod}$-$D_{2\text{-}E}$.

Table S2. Important electronic excited states and their NTOs analysis for **1**$_{mod}$-D_{2h}, **1**$_{mod}$-D_2 and **1**$_{mod}$-$D_{2\text{-}E}$.

Complex	Electronic transition	λ	Energy	R_{vel}	Assignment (H = HOMO, L = LUMO)
1_{mod}-D_{2h}	$S_0 \rightarrow S_1$	363.86nm	3.4075eV	0	(0.70)H→L
	$S_0 \rightarrow S_2$	310.16nm	3.9974eV	0	(0.47)H-1→L
					(0.49)H→L+1
					(-0.14)H→L+5
1_{mod}-D_2	$S_0 \rightarrow S_1$	366.76nm	3.3806eV	7.5272	(0.70)H→L
	$S_0 \rightarrow S_2$	310.45nm	3.9937 eV	1.3258	(0.47)H-1→L
					(0.50)H→L+1
					(-0.14)H→L+5
1_{mod}-$D_{2\text{-}E}$	$S_0 \rightarrow S_1$	366.76nm	3.3806eV	-7.5272	(0.70)H→L
	$S_0 \rightarrow S_2$	310.45nm	3.9937 eV	-1.3258	(0.47)H-1→L
					(0.50)H→L+1
					(-0.14)H→L+5

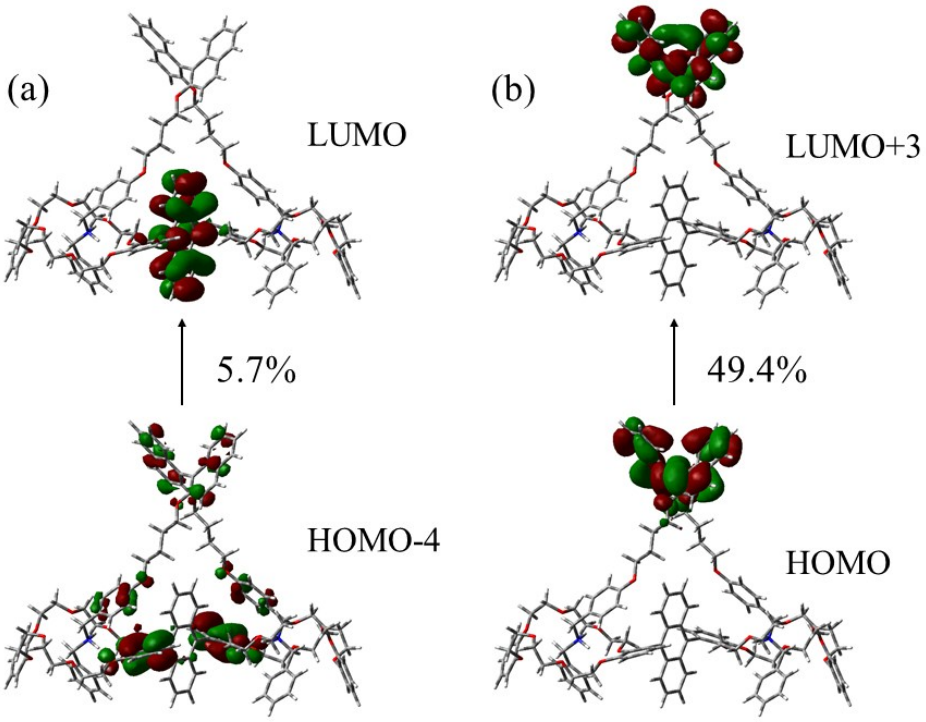

Figure S24. The transitions of (a) the CT in S_2 and (b) the main LE in S_4.

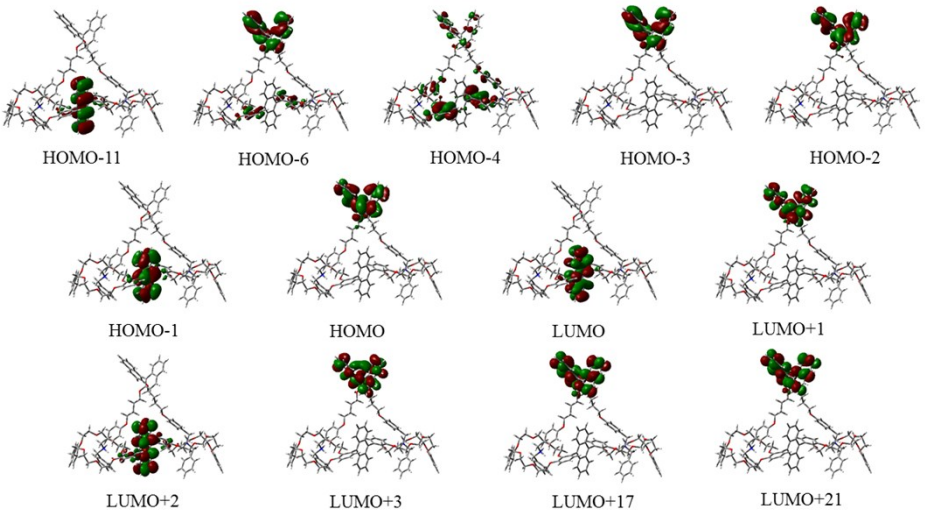

Figure S25. The MOs participated in the transition of (*R*)-**2**@**1**.

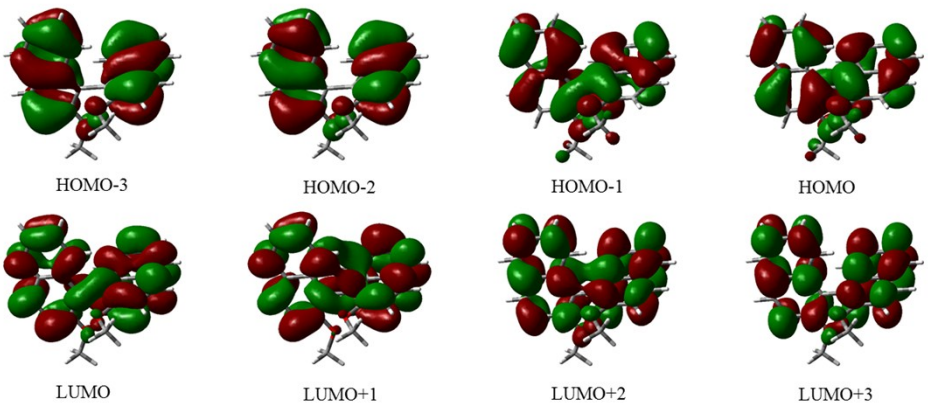

Figure S26. The MOs participated in the transition of (*R*)-**2**mod.

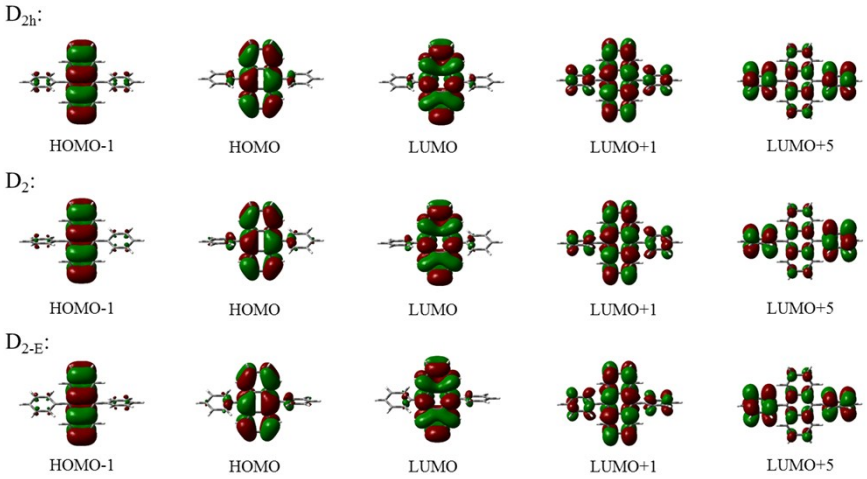

Figure S27. The MOs participated in the transition of $\mathbf{1}_{mod}$-D_{2h}, $\mathbf{1}_{mod}$-D_2 and $\mathbf{1}_{mod}$-$D_{2\text{-}E}$.

References

[a] W. Jiang, K. Nowosinski, N. L. Löw, E. V. Dzyuba, F. Klautzsch, A. Schäfer, J. Huuskonen, K. Rissanen and C. A. Schalley, *J. Am. Chem. Soc.*, 2012, **134**, 1860-1868.

[b]. M. J. Frisch, G. W. Trucks, H. B. Schlegel, G. E. Scuseria, M. A. Robb, J. R. Cheeseman, G. Scalmani, V. Barone, G. A. Petersson, H. Nakatsuji, X. Li, M. Caricato, A. V. Marenich, J. Bloino, B. G. Janesko, R. Gomperts, B. Mennucci, H. P. Hratchian, J. V. Ortiz, A. F. Izmaylov, J. L. Sonnenberg, D. Williams-Young, F. Ding, F. Lipparini, F. Egidi, J. Goings, B. Peng, A. Petrone, T. Henderson, D. Ranasinghe, V. G. Zakrzewski, J. Gao, N. Rega, G. Zheng, W. Liang, M. Hada, M. Ehara, K. Toyota, R. Fukuda, J. Hasegawa, M. Ishida, T. Nakajima, Y. Honda, O. Kitao, H. Nakai, T. Vreven, K. Throssell, J. A. Montgomery, Jr., J. E. Peralta, F. Ogliaro, M. J. Bearpark, J. J. Heyd, E. N. Brothers, K. N. Kudin, V. N. Staroverov,

T. A. Keith, R. Kobayashi, J. Normand, K. Raghavachari, A. P. Rendell, J. C. Burant, S. S. Iyengar, J. Tomasi, M. Cossi, J. M. Millam, M. Klene, C. Adamo, R. Cammi, J. W. Ochterski, R. L. Martin, K. Morokuma, O. Farkas, J. B. Foresman, and D. J. Fox, Gaussian 16, Revision A.03, Gaussian, Inc., Wallingford, CT, 2016.

[c]. (a) A. D. Becke, *J. Cherm. Phys.*, 1993, **98**, 5648-5652; (b) A. D. Becke, *J. Chem. Phys.*, 1993, **98**, 1372-1377; (c) K. Raghavachari, *Theor. Chem. Acc.,* 2000, **103**, 361-363.

[d]. (a) S. Grimme, J. Antony, S. Ehrlich and H. Krieg, *J. Chem. Phys.*, 2010, **132**, 154104; (b) S. Grimme, *J. Comput. Chem.*, 2006, **27**, 1787-1799.

[e]. P. C. Hariharan and J. A. Pople, *Theor. Chim. Acta*, 1973, **28**, 213-222.

[f]. (a) Y. Zhao and D. G. Truhlar, *Acc. Chem. Res.*, 2008, **41**, 157-167; bY. Zhao and D. G. Truhlar, *Theor. Chem. Acc.*, 2008, **120**, 215-241.

[g]. (a) B. Mennucci and J. Tomasi, *J. Chem. Phys.*, 1997, **106**, 5151-5158; (b) V. Barone and M. Cossi, *J. Phys. Chem. A*, 1998, **102**, 1995-2001.

[h]. C. Y.Legault, CYLview, 1.0b, Université de Sherbrooke, Sherbrooke, Quebec, Canada, 2009, http://www.cylview.org.